

Towards a Better Understanding of Cosmic Chronometers: A new measurement of $H(z)$ at $z \sim 0.7$

NICOLA BORGHI ^{1,2} MICHELE MORESCO ^{1,2} AND ANDREA CIMATTI ^{1,3}

¹*Dipartimento di Fisica e Astronomia “Augusto Righi”, Alma Mater Studiorum Università di Bologna, via Piero Gobetti 93/2, I-40129 Bologna, Italy*

²*INAF - Osservatorio di Astrofisica e Scienza dello Spazio di Bologna, via Piero Gobetti 93/3, I-40129 Bologna, Italy*

³*INAF - Osservatorio Astrofisico di Arcetri, Largo E. Fermi 5, I-50125, Firenze, Italy*

Submitted to ApJL

ABSTRACT

In this work, we analyze the stellar ages obtained from a combination of Lick indices in [Borghi et al. \(2021\)](#) for 140 massive and passive galaxies selected in the LEGA-C survey. The median estimated age-redshift relation is used to obtain a new direct measurement of $H(z)$ with the cosmic chronometers approach without any cosmological model assumption. We thoroughly study the main systematics involved in this analysis, including the choice of Lick indices combination, the binning method, the assumed stellar population model, and the adopted star formation history; these effects are included in the total error budget, obtaining $H(z = 0.75) = 98.8 \pm 33.6$ km/s/Mpc. In parallel, we also propose a simple framework, based on a cosmological model, to describe the age-redshift relations in the context of galaxy downsizing. This allows us to derive constraints on the Hubble constant H_0 and the galaxy formation time. Our results add new fundamental elements to the cosmic chronometers approach by joining the detailed study of stellar populations of individual passive galaxies with the study of the expansion history of the Universe and show its potential in the light of upcoming spectroscopic surveys.

Keywords: Observational cosmology (1146) — Cosmological evolution (336) — Galaxy ages (576) — Hubble constant (758)

1. INTRODUCTION

In the precision cosmology era, independent cosmological probes are fundamental to keep their systematics under control, shed light in the current tensions between different measurements of cosmological parameters, and, ultimately, improve the accuracy of these measurements. Recently, much effort has been devoted to understanding the $\sim 4\sigma$ tension between the value of the Hubble constant H_0 measured in the local Universe and the one inferred from the Cosmic Microwave Background (CMB) analysis (see [Verde et al. 2019](#); [Valentino et al. 2021](#)). If confirmed, this difference would require an extension to the ‘vanilla’ 6-parameter Λ CDM model, introducing new physics at play in the early and/or late epochs. In

this context, a cosmological model-independent reconstruction of the expansion history of the Universe can play a crucial role. With the minimal assumption of a Friedmann-Lemaître-Robertson-Walker (FLRW) metric, the Hubble parameter $H(z)$ is related to the differential aging of the Universe dt_U as a function of redshift z by the following equation:

$$H(z) = -\frac{1}{1+z} \frac{dz}{dt_U}. \quad (1)$$

The idea of using a homogeneous population of astrophysical objects to trace dt_U , i.e. *cosmic chronometers* (CC), came from [Jimenez & Loeb \(2002\)](#), who proposed massive passively evolving galaxies as ideal CC candidates. Many observational studies revealed that these galaxies build up their mass at high redshift ($z \gtrsim 2$) over short timescales (< 1 Gyr) exhausting almost completely their gas reservoir in the very first stages of their life and hence evolve passively to the present

age (e.g. Cimatti et al. 2004; Treu et al. 2005; Renzini 2006; Pozzetti et al. 2010; Thomas et al. 2010). However, while redshifts can be measured with high precision (up to 0.1% with spectroscopic observations), age-dating galaxies is challenged by the complex reconstruction of their star formation history (SFH), and by intrinsic degeneracies within stellar population parameters (e.g. stellar age and chemical composition, see Conroy 2013).

In the first works, CCs were selected as red massive galaxies and analyzed with stellar population models to both detect those evolving passively, and derive their ages (Jimenez 2003; Simon et al. 2005; Stern et al. 2010). A different approach was introduced by Moresco et al. (2011), who proposed to use a direct observable, the spectral break at 4000 Å rest-frame (hereafter D4000), to trace the differential age evolution of carefully selected samples of passive galaxies. In fact, the D4000 is linearly correlated (within the considered regimes) with the age of the stellar population, so that the dz/dt_U can be expressed as $A \times dz/dD4000$, where the calibration factor A encapsulates stellar population modeling dependencies, such as metallicity and star formation history. To date, the majority of $H(z)$ measurements are based on this method. The other available measurements were made analyzing the ages of luminous red galaxies with the full spectral fitting technique (using, in particular, the Ulyss code, Zhang et al. 2014; Ratsimbazafy et al. 2017).

In the previous paper (Borghi et al. 2021, hereafter Paper I), we derived robust stellar population properties for individual passive galaxies at $z \sim 0.7$ taking advantage of the high-quality spectroscopy of the Large Early Galaxy Astrophysics Census (LEGA-C, van der Wel et al. 2016; Straatman et al. 2018) using an optimized set of spectral (Lick) indices.

In this Letter, we take advantage of the derived age-redshift relation to obtain a new $H(z)$ estimate at $z \simeq 0.75$. This enables us, for the first time, to study the stellar population properties (age, metallicity $[Z/H]$, and α -enhancement $[\alpha/Fe]$) of a vast sample of individual cosmic chronometers and use them to constrain the expansion history of the Universe. We also use these data to extract information on H_0 and $\Omega_{m,0}$ jointly with the typical formation time of these systems.

The $H(z)$ measurement provided in this work does not rely on the assumption of a cosmological model, but only on the minimal assumption of the FLRW metric (Eq. 1). For purely reference values and illustrative purposes, we adopt a ‘737’ cosmology ($H_0 = 70$ km/s/Mpc, $\Omega_{m,0} = 0.3$, $\Omega_{\Lambda,0} = 0.7$).

2. DATA

The present work relies on the detailed stellar population analysis of selected massive and passive galaxies carried out in Paper I, enabled by the high signal-to-noise ratio ~ 20 and resolution of $R \sim 3500$ of the LEGA-C DR2 spectra (van der Wel et al. 2016; Straatman et al. 2018). These galaxies have a typical stellar velocity dispersion of $\sigma_* \sim 215$ km/s and stellar mass of $\log(M_*/M_\odot) \sim 11$. We obtained robust stellar age, metallicity $[Z/H]$, and $[\alpha/Fe]$ measurements for 140 galaxies at $0.6 \lesssim z \lesssim 0.9$, comparing an optimized set of spectral absorption features ($H\delta_A$, CN_1 , CN_2 , $Ca4227$, $G4300$, $H\gamma_A$, $H\gamma_F$, $Fe4383$, $Fe4531$, C_24668 , hereafter *baseline*) with the Thomas et al. (2011) models. These models, that we consider for our constraints as vastly done in the literature, assume a single-burst star formation history (SFH). A more realistic SFH is expected to be more complex. However, the analysis of several indicators, including color-color, star formation rate-mass diagrams, and spectroscopic features as the novel CaII H/K diagnostic (Moresco et al. 2018), confirm that these galaxies are passively evolving, and must have formed over very short time scales (Paper I). We will better quantify the impact of this assumption in Sect. 3.1.

The galaxies are divided into two stellar velocity dispersion sub-samples using their median $\langle\sigma_*\rangle = 215$ km/s. For each σ_* regime, we evaluate the median age in four narrow redshift bins (see Fig. 1, *upper panel*). The constant bin width $\Delta z \simeq 0.075$ corresponds to ~ 0.4 Gyr difference in cosmic time, which is also the average age uncertainty. To each bin, we associate an uncertainty computed as the median standard error (NMAD, Hoaglin et al. 1983). The two resulting age- z relations for the higher and lower σ_* regime are approximately parallel and with an offset of $\Delta\text{age} \simeq 0.5$ Gyr. This is consistent with the mass-downsizing scenario, for which more massive galaxies formed earlier and faster.

We stress here the utmost importance of avoiding any cosmological prior in the age determination, as done in Paper I; while this kind of prior is commonly used in the literature to reduce the degeneracies between parameters, in the CC method is fundamental not to use it to avoid introducing circularity in the analysis, with the risk of retrieving the same cosmological parameters adopted as priors.

3. THE DIRECT APPROACH: $H(z)$ MEASUREMENT

In the cosmic chronometers approach, the Hubble parameter $H(z)$ can be derived directly and without any

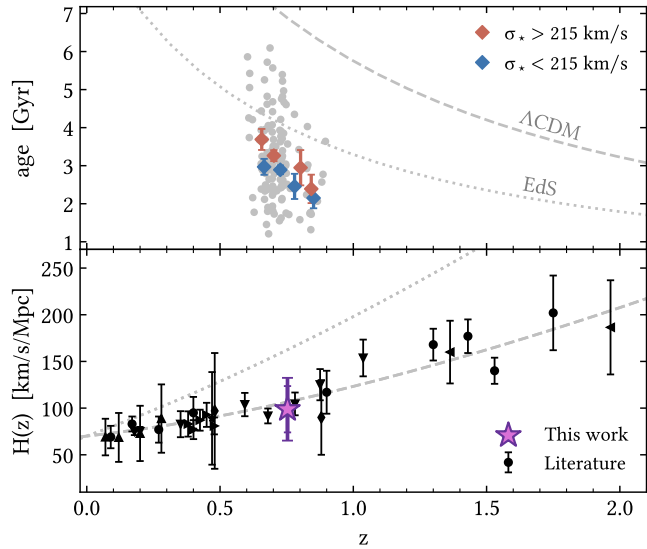


Figure 1. *Upper panel:* median binned age-redshift relation for 140 passive galaxies analyzed in Borghi et al. (2021) (gray points) divided into higher (red) and lower (blue) σ_* regimes. *Lower panel:* $H(z)$ measurement (violet star) with statistical (inner errorbar) and total (outer errorbar) uncertainties. Black points are literature data from: Simon et al. 2005 (\bullet), Stern et al. 2010 (\blacklozenge), Moresco et al. 2012 (\blacktriangledown), Zhang et al. 2014 (\blacktriangle), Moresco 2015 (\blacktriangleleft), Moresco et al. 2016 (\blacktriangleright), Ratsimbazafy et al. 2017 (\blacksquare). Gray lines are theoretical relations for a standard Λ CDM (dashed) and Einstein-de Sitter (dotted) cosmology.

Table 1. Hubble parameter measurements

Sample	Bins	z_{eff}	$H(z_{\text{eff}})$	σ_{stat}	# gal.
			km/s/Mpc	km/s/Mpc	
Lower σ_*	1 & 3	0.72	126.3	96.4	20
	2 & 4	0.79	92.0	36.3	50
Higher σ_*	1 & 3	0.73	111.0	80.7	21
	2 & 4	0.77	88.6	40.6	49
Joint	all	0.75	98.8	24.8	140

cosmological assumptions from the differential age evolution of CC, $\Delta\text{age}_{\text{CC}}$, within a redshift interval Δz (Eq. 1). The quantity $\Delta z/\Delta\text{age}_{\text{CC}}$ is measured from the median age-redshift relation between the i -th and the $i+2$ -th points for each σ_* sub-sample, and is defined at an effective redshift of $z_{\text{eff}} = (z_i + z_{i+2})/2$. The choice to use alternate points is to ensure that the evolution in age over the assumed redshift intervals Δz (~ 0.4 Gyr of cosmic time) is larger than the statistical scatter, but at the same time sufficiently small to minimize possible systematic effects (see Moresco et al. 2012). With this

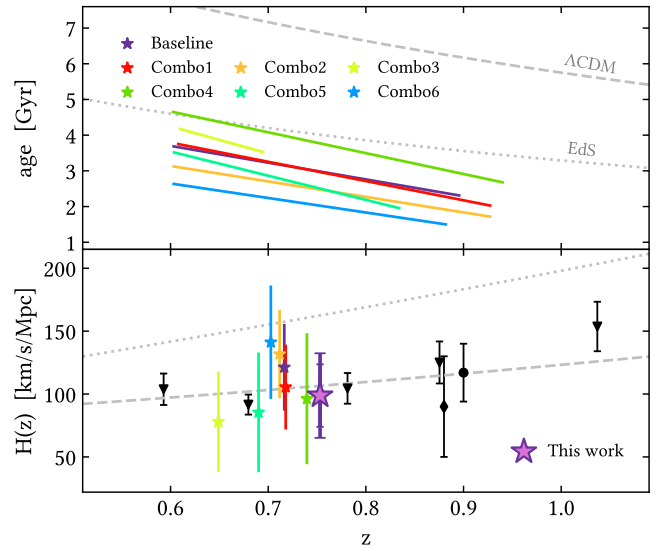


Figure 2. Same as Fig. 1, but showing the results obtained with linear fits to the unbinned age- z relations for different combinations of indices used in the analysis (as presented in Borghi et al. 2021). Gray lines are theoretical relations for a standard Λ CDM (dashed) and Einstein-de Sitter (dotted) cosmology and are shown for visual inspection purposes only. We note that the EdS model predicts a much flatter slope compared to the ones of the data, which are instead more compatible with a Λ CDM scenario, as also confirmed the $H(z)$ measurements.

bin choice, we obtain four $H(z)$ estimates listed in Table 1.

We find that the results for lower and higher σ_* regimes are in very good agreement, with their mean values being within 0.1σ , confirming the idea that these two sub-populations are tracing the same underlying cosmology. Since all the four measurements are independent from each other, we combine them using a variance-weighted average, obtaining $H(z = 0.75) = 98.8 \pm 24.8$ (*stat*) km/s/Mpc at 68% C.L. (Fig. 1, *lower panel*). Our measurement is perfectly consistent with the values estimated with different CC datasets and methods. In particular, the most comparable measurements at this redshift are both from Moresco et al. (2012) using the D4000 method. Our value lies in between their $H(z = 0.68) = 91.6 \pm 8.0$ km/s/Mpc and $H(z = 0.78) = 104.5 \pm 12.2$ km/s/Mpc, differing only by $+0.3\sigma$ and -0.2σ , respectively.

3.1. Assessing the systematic uncertainties

In this section, we explore the main sources of systematic uncertainties in our work. The total uncertainty on $H(z)$ will be computed by adding in quadrature the systematic and statistical contributions.

Dependence on Lick index sets—In [Paper I](#), we studied how different combinations of absorption features impact the derived stellar population parameters. Here, we use this dataset to study the effect of this choice on the age-redshift slope and the final $H(z)$ value. The *baseline* index combination was devised to maximize the number of indices to be measured given the redshift and wavelength coverage of the various galaxies; moreover, any other index set provides age constraints for fewer objects (down to a dozen for the worst case) and binning them is not always an option. For this reason, to assess this systematic effect we estimate $\Delta z/\Delta \text{age}_{CC}$ and its associated uncertainty from the inverse slope of the age-redshift relation obtained with a simple linear regression. Results are shown in [Fig. 2](#) (see [appendix C](#) of [Paper I](#) for index set definitions).

We notice that different combinations of indices can provide systematically different absolute age estimates, ranging within ± 1 Gyr. However, we find that the $H(z)$ estimates are consistent with each other and with the more statistically rigorous value obtained with the median binning within 0.4σ , on average. These results clearly highlight the advantages of CC being a *differential approach*; in other words, the absolute age calibration that might be obtained in different analyses does not significantly affect the final $H(z)$ value, but only the normalization of the age- z relation.

Dependence on the binning—We verify that our result is robust against different redshift binning schemes and adopted estimators. In particular, by using from two up to six redshift intervals, or/and the mean instead of the median age, $H(z)$ results are on average within 0.5σ with respect to the baseline. We do not use weighted averages, because in [Paper I](#) we found that the stellar population analysis intrinsically yields higher uncertainties for older galaxies and this would bias the final age-redshift slope. Finally, we also repeat the analysis using equally populated (~ 20 objects) redshift bins. This method improves the statistics of single bins at the expense of smaller leverage in redshift. Even in this case, we obtain values in good agreement, with an average difference of 0.5σ .

Dependence on the SPS model—The choice of the stellar population model plays a major role in the overall systematics of the CC approach. Quantitatively, [Moresco et al. \(2020\)](#) measured an average contribution of $\sim 7\%$ on the final uncertainty of $H(z)$ using the D4000 method. To assess this effect in our work, we repeat the entire analysis by adopting the α -MILES models by [Vazdekis et al. \(2015\)](#). The detailed analysis is presented in [Appendix A.1](#). We find that the $H(z)$

measurements obtained with the assumption of a different SPS model are consistent with the *baseline* within 0.6σ , on average.

Dependence on a more extended SFH—In all the previous analyses, we assume single-burst star formation histories (SFH). This is justified by the accurate selection of passive systems which maximizes the presence of galaxies with coeval SFH concentrated at early cosmic epochs. Here, we assess the effect of assuming a more extended SFH $\propto \exp(t/\tau)$, i.e. exponentially declining with a characteristic timescale τ . Also in this case, the detailed analysis is presented in [Appendix A.2](#). As expected from the sample selection, we confirm very short SFHs with a typical $\tau \lesssim 0.4$ Gyr. By analyzing the slopes of the age-redshift relations obtained with these more extended SFHs, we find that the final $H(z)$ measurements differ by only 0.4σ , on average, with respect to the *baseline*.

Final $H(z)$ measurement—To summarize, we have collected a total of 15 measurements of $H(z)$ by varying the Lick index set, the redshift binning method, the stellar population synthesis model, and the assumed SFH. With this dataset, we compute a systematic error (obtained from the standard deviation) of 22.7 km/s/Mpc with respect to our baseline result. This value has been added in quadrature to the statistical error, obtaining as a final result:

$$H(z = 0.75) = 98.8 \pm 33.6 \text{ km/s/Mpc} \quad (2)$$

at 68% C.L., where the contribution to the systematic error is almost equally distributed between the various components, being about 1/3 for the Lick index combination, 1/4 for the binning and for the SPS model, and 1/6 for the SFH. This is the first $H(z)$ measurement based on the analysis of absorption features of individual passive galaxies, confirming that it is possible to jointly study their stellar population and use them to derive cosmological constraints. Moreover, this measurement is obtained in a poorly mapped region of the redshift space that is crucial to reconstruct the expansion history of the Universe. In fact, for the assumed fiducial cosmology the transition between a decelerated and accelerated expansion, or *transition redshift*, occurs at $z_t = 0.67$.

4. COSMOLOGICAL CONSTRAINTS FROM THE ANALYSIS OF AGE-REDSHIFT RELATIONS

The age-redshift relations can be used to set constraints on the Hubble constant H_0 , and other cosmological parameters (e.g. [Jimenez et al. 2019](#); [Vagnozzi et al. 2021](#)). A recent measurement of H_0 in the local

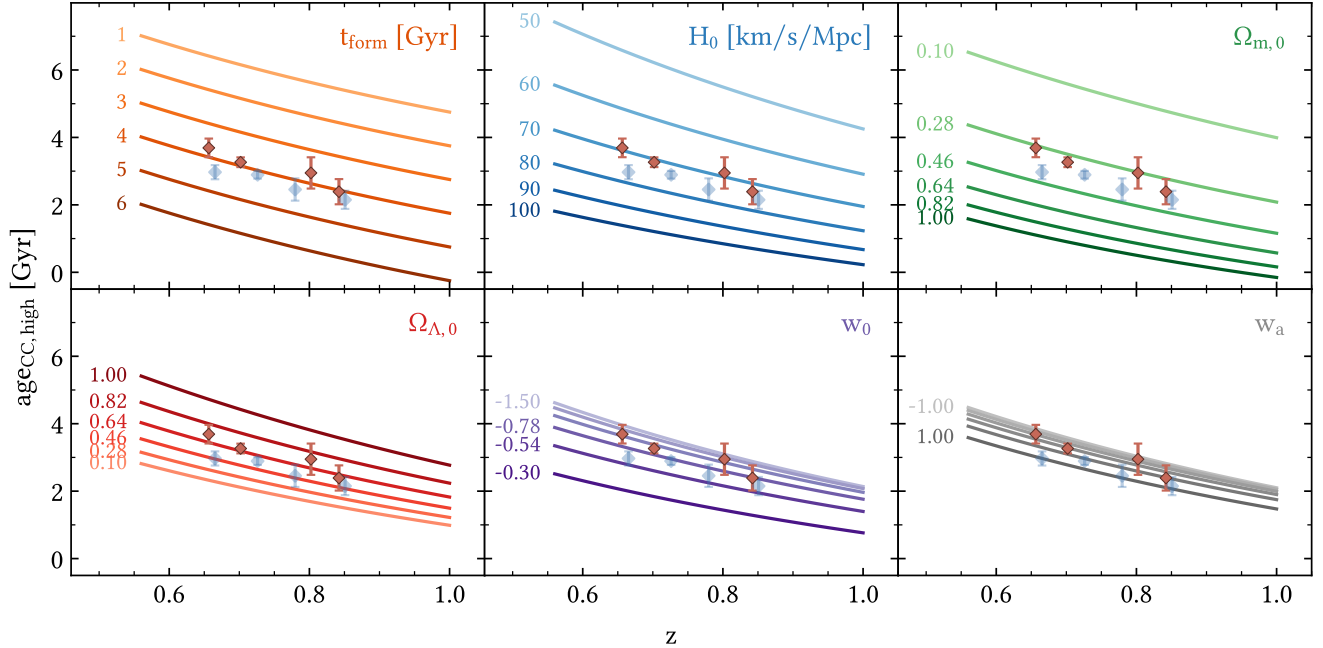


Figure 3. Theoretical age-redshift relations for the high- σ_* sub-sample of cosmic chronometers. Each panel shows the effect of varying each parameter to the labeled values. Red diamonds are median binned data for the high- σ_* sub-sample of cosmic chronometers from Paper I. For illustrative purposes, we also show the data points of the lower σ_* sub-sample (blue diamonds), which are, on average, about 0.5 Gyr younger. When not varied, the parameters are set to the following fiducial values: $t_{form} = 3.8$ Gyr, $H_0 = 70$ km/s/Mpc, $\Omega_{m,0} = 0.3$, $\Omega_{\Lambda,0} = 0.7$, $w_0 = -1$, and $w_a = 0$.

Universe has been obtained by Riess et al. (2021) using the luminosity distances of type Ia supernovae calibrated with Cepheid variable stars, $H_0 = 73.2 \pm 1.3$ km/s/Mpc at 68% C.L. This value is at 4σ tension with the Λ CDM model-dependent value inferred from the CMB, $H_0 = 67.36 \pm 0.54$ km/s/Mpc (Planck Collaboration 2018, TT,TE,EE+lowE+lensing).

In this Section, we propose a simple scheme to derive cosmological parameters from the age-redshift relations of different sub-samples of CCs divided by their stellar velocity dispersion σ_* , in the context of a downsizing evolution (more massive galaxies formed earlier).

4.1. The model

The age of the Universe as a function of redshift, $t_U(z)$, can be predicted from cosmological models. Here we assume that the late-time expansion history is described by a flat $w_0 w_a$ CDM universe, where the dark energy equation of state can vary as a function of cosmic time under the CPL parameterization, $w(z) = w_0 + w_a(z/(1+z))$ (Chevallier & Polarski 2001; Linder 2003):

$$t_U(z) = \frac{1}{H_0} \int_z^\infty \frac{dz'}{(1+z')E(z')}, \quad (3)$$

where H_0 is the Hubble parameter in the local Universe and:

$$E(z) = \sqrt{\Omega_{m,0}(1+z)^3 + \Omega_{\Lambda,0}(1+z)^{3(1+w_0+w_a)}e^{-3w_a\frac{z}{1+z}}}, \quad (4)$$

where $\Omega_{m,0}$ and $\Omega_{\Lambda,0}$ are the adimensional energy density parameters for matter and dark energy respectively (radiation is not considered since its contribution is negligible in the late Universe). Given the inverse relationship between $t_U(z)$ and H_0 , lower limits on $t_U(z)$ from the ages of the oldest objects would determine upper limits on the local H_0 value. Recently, this method has been applied by Vagnozzi et al. (2021) to obtain constraints on H_0 from galaxies and quasars observed up to $z \sim 8$.

Galaxy formation occurs after a time t_{form} from the Big-Bang, which could in principle vary with redshift depending on the considered sample. However, CCs are a population of objects selected to be very coeval in formation time. Therefore, their age- z relation can be written as:

$$\text{age}_{CC}(z) = t_U(z) - t_{form}. \quad (5)$$

According to the downsizing scenario, galaxy mass is a main driver of galaxy formation and evolution, with more massive galaxies forming their stars at earlier cosmic epochs with respect to less massive ones. For this

reason, multiple parallel age-redshift relations for different σ_* populations are expected (and actually visible in the current dataset). Therefore, we use both the lower and higher σ_* sub-samples as homogeneous tracers of the age of the Universe by assuming a constant offset in formation time Δt_f computed as the mean age difference. We take as a reference the higher σ_* age- z relation $\text{age}_{CC,high}(z)$, so that $\text{age}_{CC,low}(z) = \text{age}_{CC,high}(z) - \Delta t_f$. In Fig. 3 we illustrate the dependency of $\text{age}_{CC,high}(z)$ on t_{form} and the cosmological parameters by varying one parameter at a time.

As expected from Eq. 3, similar age- z trends can be found increasing t_{form} (hence t_U) and decreasing H_0 (and vice-versa). A less evident anti-correlation is observed between $H_0 - \Omega_{m,0}$ and $\Omega_{m,0} - \Omega_{\Lambda,0}$. The latter is orthogonal to the one present in CMB only data, so it is interesting to explore this method as an independent probe to eventually obtain more stringent constraints when combining the two (see e.g. Moresco et al. 2016). Finally, it is clear that with the current data it is not possible to set tight constraints on the dark energy equation of state parameters w_0 and w_a due to their smaller effect on $\text{age}(z)$.

In our analysis, we therefore assume a flat Λ CDM universe ($\Omega_{\Lambda,0} = 1 - \Omega_{m,0}$, $w_0 = -1$, $w_a = 0$), so that the final model is described by 3 parameters, $\theta = (t_{form}, H_0, \Omega_{m,0})$. We constrain these parameters by using the affine-invariant Monte Carlo Markov Chain sampler `emcee` (Foreman-Mackey et al. 2019), assuming a Gaussian likelihood function $\propto e^{-\chi^2/2}$. Priors are set to uniform, non-informative, $H_0 \sim \mathcal{U}(0, 150)$ km/s/Mpc, $\Omega_{m,0} \sim \mathcal{U}(0.01, 0.99)$, and $t_{form} \sim \mathcal{U}(1, 10)$ Gyr. The final values and associated uncertainties are defined as the cumulative mean and 1σ values of the marginalized posterior distributions.

4.2. Results

The results are shown in Fig. 4. We obtain $H_0 = 72_{-19}^{+27}$ km/s/Mpc, $\Omega_{m,0} = 0.38_{-0.23}^{+0.36}$, and $t_{form} = 3.2_{-1.3}^{+1.8}$ Gyr. Given the large uncertainties and the small redshift range sampled, our current result is in agreement with both early and late-Universe H_0 determinations; moreover, this method is limited by the intrinsic degeneracies between the parameters shown in Fig. 3. We note, however, that these constraints can be significantly improved by increasing the redshift leverage and accuracy of the data, as, for example, could be done by analyzing massive and passive galaxies from proposed spectroscopic missions, such as the ATLAS probe (Wang et al. 2019). Differently from the standard CC method presented in Sec. 3, this relies on absolute ages estimates,

and therefore requires an accurate calibration and a homogeneous analysis between different samples.

We also repeat the analysis assuming a Gaussian prior on $\Omega_{m,0} \sim \mathcal{N}(0.316, 0.007)$ based on (Planck Collaboration 2018) TT,TE,EE+lowE+lensing results. In this case, we obtain $H_0 = 77_{-17}^{+20}$ km/s/Mpc, and $t_{form} = 3.0_{-1.2}^{+1.7}$ Gyr with a significant degeneracy between the two parameters.

5. CONCLUSIONS

In this Letter, we build upon our previous analysis of stellar population parameters of 140 individual passive galaxies at intermediate redshift (Borghi et al. 2021) to derive cosmological constraints using the cosmic chronometer approach.

1. We derive a direct and cosmology-independent estimate of the Hubble parameter $H(z = 0.75) = 98.8 \pm 33.6$ km/s/Mpc including both statistical and systematic uncertainties. The latter are obtained by varying the indices adopted to estimate mean stellar ages, the binning scheme, and by assuming different stellar population synthesis models and star formation histories.
2. We propose a simple model to analyze age-redshift relations of CC at different stellar velocity dispersion σ_* regimes. Assuming a flat Λ CDM universe, we obtain $H_0 = 72_{-19}^{+27}$ km/s/Mpc, and a typical formation time of $t_{form} = 3.2_{-1.3}^{+1.8}$ Gyr after the Big Bang for the high σ_* (> 215 km/s) sub-sample.

This work demonstrates that it is possible to extend the cosmic chronometer approach by performing a detailed study of galaxy stellar populations with spectral indices, providing at the same time information on galaxy evolution and cosmology. In view of the extremely interesting constraints to H_0 from gravitational waves (e.g. GW170817, Abbott et al. 2017) and of the improvements expected in the near future, an important step forward will be the combination of CC and GW analyses, in order to reconstruct for the first time a cosmology-independent expansion history of the Universe from $z \sim 0$ to $z \sim 2$.

- 1 This work is based on data products from observa-
- 2 tions made with ESO Telescopes at the La Silla Paranal
- 3 Observatory under program ID 194.AF2005(A-N). We
- 4 thank the LEGA-C team for making their dataset pub-
- 5 lic. NB and MM acknowledge support from MIUR,
- 6 PRIN 2017 (grant 20179ZF5KS). MM and AC acknowl-
- 7 edge the grants ASI n.I/023/12/0 and ASI n.2018-23-
- 8 HH.0. AC acknowledges the support from grant PRIN
- 9 MIUR 2017 - 20173ML3WW_001.

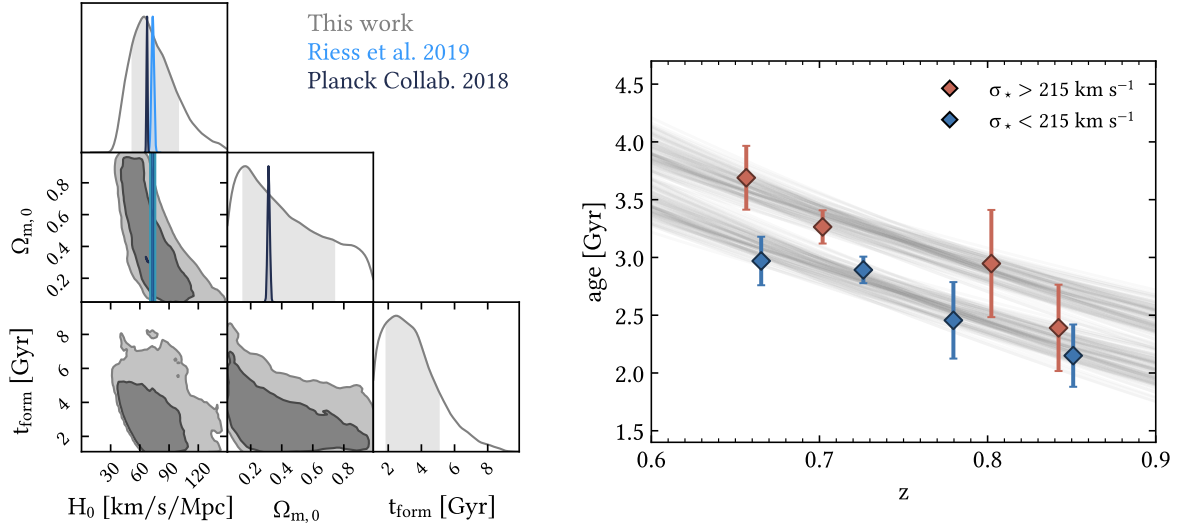


Figure 4. Constraints from age-redshift relations assuming a flat Λ CDM model. *Left:* Corner plot for H_0 , $\Omega_{m,0}$, t_{form} , showing 1σ (darker shade) and 2σ (lighter shade) regions. Vertical shaded bands are the cumulative 1σ confidence regions. Our results are compared with those from Riess et al. (2021) and Planck Collaboration (2018, TT,TE,EE+lowE+lensing). *Right:* Resulting fits (gray lines) to the observed age redshift relations (diamonds).

Software: CHAINCONSUMER (Hinton 2016), COSMOBOLOGNALIB (Marulli et al. 2016), EMCEE (Foreman-Mackey et al. 2019), MATPLOTLIB (Hunter 2007),

NUMPY (Harris et al. 2020), PYLICK (Borghini et al. 2021)

REFERENCES

- Abbott, B. P., Abbott, R., Abbott, T. D., et al. 2017, Nature, 551, 85, doi: [10.1038/nature24471](https://doi.org/10.1038/nature24471)
- Borghini, N., Moresco, M., Cimatti, A., et al. 2021
- Chevallier, M., & Polarski, D. 2001, International Journal of Modern Physics D, 10, 213, doi: [10.1142/S0218271801000822](https://doi.org/10.1142/S0218271801000822)
- Cimatti, A., Daddi, E., Renzini, A., et al. 2004, Nature, 430, 184, doi: [10.1038/nature02668](https://doi.org/10.1038/nature02668)
- Conroy, C. 2013, Annual Review of Astronomy and Astrophysics, 51, 393, doi: [10.1146/annurev-astro-082812-141017](https://doi.org/10.1146/annurev-astro-082812-141017)
- Falc3n-Barroso, J., S3nchez-Bl3zquez, P., Vazdekis, A., et al. 2011, Astronomy & Astrophysics, 532, A95, doi: [10.1051/0004-6361/201116842](https://doi.org/10.1051/0004-6361/201116842)
- Foreman-Mackey, D., Farr, W., Sinha, M., et al. 2019, Journal of Open Source Software, 4, 1864, doi: [10.21105/joss.01864](https://doi.org/10.21105/joss.01864)
- Gavazzi, G., Bonfanti, C., Sanvito, G., Boselli, A., & Scodreggio, M. 2002, ApJ, 576, 135, doi: [10.1086/341730](https://doi.org/10.1086/341730)
- Harris, C. R., Millman, K. J., van der Walt, S. J., et al. 2020, Nature, 585, 357, doi: [10.1038/s41586-020-2649-2](https://doi.org/10.1038/s41586-020-2649-2)
- Hinton, S. 2016, The Journal of Open Source Software, 1, 45, doi: [10.21105/joss.00045](https://doi.org/10.21105/joss.00045)
- Hoaglin, D. C., Mosteller, F., & Tukey, J. W. 1983, Understanding Robust and Exploratory Data Analysis (Wiley). <https://books.google.it/books?id=FRnvAAAAMAAJ>
- Hunter, J. D. 2007, Computing in Science and Engineering, 9, 90, doi: [10.1109/MCSE.2007.55](https://doi.org/10.1109/MCSE.2007.55)
- Jimenez, R. 2003, New Astronomy Reviews, 47, 761, doi: [10.1016/j.newar.2003.07.004](https://doi.org/10.1016/j.newar.2003.07.004)
- Jimenez, R., Cimatti, A., Verde, L., Moresco, M., & Wandelt, B. 2019, JCAP, 2019, 043, doi: [10.1088/1475-7516/2019/03/043](https://doi.org/10.1088/1475-7516/2019/03/043)
- Jimenez, R., & Loeb, A. 2002, The Astrophysical Journal, 573, 37, doi: [10.1086/340549](https://doi.org/10.1086/340549)
- Linder, E. V. 2003, Physical Review Letters, 90, 091301, doi: [10.1103/physrevlett.90.091301](https://doi.org/10.1103/physrevlett.90.091301)
- Marulli, F., Veropalumbo, A., & Moresco, M. 2016, Astronomy and Computing, 14, 35, doi: [10.1016/j.ascom.2016.01.005](https://doi.org/10.1016/j.ascom.2016.01.005)
- Moresco, M. 2015, Monthly Notices of the Royal Astronomical Society: Letters, 450, L16, doi: [10.1093/mnrasl/slv037](https://doi.org/10.1093/mnrasl/slv037)
- Moresco, M., Jimenez, R., Cimatti, A., & Pozzetti, L. 2011, Journal of Cosmology and Astroparticle Physics, 2011, 045, doi: [10.1088/1475-7516/2011/03/045](https://doi.org/10.1088/1475-7516/2011/03/045)

- Moresco, M., Jimenez, R., Verde, L., Cimatti, A., & Pozzetti, L. 2020, *ApJ*, 898, 82, doi: [10.3847/1538-4357/ab9eb0](https://doi.org/10.3847/1538-4357/ab9eb0)
- Moresco, M., Jimenez, R., Verde, L., et al. 2018, *ApJ*, 868, 84, doi: [10.3847/1538-4357/aae829](https://doi.org/10.3847/1538-4357/aae829)
- Moresco, M., Cimatti, A., Jimenez, R., et al. 2012, *JCAP*, 2012, 006, doi: [10.1088/1475-7516/2012/08/006](https://doi.org/10.1088/1475-7516/2012/08/006)
- Moresco, M., Pozzetti, L., Cimatti, A., et al. 2016, *Journal of Cosmology and Astroparticle Physics*, 2016, 014, doi: [10.1088/1475-7516/2016/05/014](https://doi.org/10.1088/1475-7516/2016/05/014)
- Pietrinferni, A., Cassisi, S., Salaris, M., & Castelli, F. 2006, *The Astrophysical Journal*, 642, 797, doi: [10.1086/501344](https://doi.org/10.1086/501344)
- Planck Collaboration. 2018, *A&A*, doi: [10.1051/0004-6361/201833910](https://doi.org/10.1051/0004-6361/201833910)
- Pozzetti, L., Bolzonella, M., Zucca, E., et al. 2010, *Astronomy & Astrophysics*, 523, A13, doi: [10.1051/0004-6361/200913020](https://doi.org/10.1051/0004-6361/200913020)
- Ratsimbazafy, A. L., Loubser, S. I., Crawford, S. M., et al. 2017, *MNRAS*, 467, 3239, doi: [10.1093/mnras/stx301](https://doi.org/10.1093/mnras/stx301)
- Renzini, A. 2006, *Annual Review of Astronomy and Astrophysics*, 44, 141, doi: [10.1146/annurev.astro.44.051905.092450](https://doi.org/10.1146/annurev.astro.44.051905.092450)
- Riess, A. G., Casertano, S., Yuan, W., et al. 2021, *ApJL*, 908, L6, doi: [10.3847/2041-8213/abdbaf](https://doi.org/10.3847/2041-8213/abdbaf)
- Simon, J., Verde, L., & Jimenez, R. 2005, *Physical Review D*, 71, doi: [10.1103/physrevd.71.123001](https://doi.org/10.1103/physrevd.71.123001)
- Stern, D., Jimenez, R., Verde, L., Kamionkowski, M., & Stanford, S. A. 2010, *JCAP*, 2010, 008, doi: [10.1088/1475-7516/2010/02/008](https://doi.org/10.1088/1475-7516/2010/02/008)
- Straatman, C. M. S., van der Wel, A., Bezanson, R., et al. 2018, *ApJS*, 239, 27, doi: [10.3847/1538-4365/aae37a](https://doi.org/10.3847/1538-4365/aae37a)
- Thomas, D., Maraston, C., & Johansson, J. 2011, *Monthly Notices of the Royal Astronomical Society*, 412, 2183, doi: [10.1111/j.1365-2966.2010.18049.x](https://doi.org/10.1111/j.1365-2966.2010.18049.x)
- Thomas, D., Maraston, C., Schawinski, K., Sarzi, M., & Silk, J. 2010, *MNRAS*, 404, 1775, doi: [10.1111/j.1365-2966.2010.16427.x](https://doi.org/10.1111/j.1365-2966.2010.16427.x)
- Treu, T., Ellis, R. S., Liao, T. X., et al. 2005, *The Astrophysical Journal*, 633, 174, doi: [10.1086/444585](https://doi.org/10.1086/444585)
- Vagnozzi, S., Pacucci, F., & Loeb, A. 2021
- Valentino, E. D., Mena, O., Pan, S., et al. 2021
- van der Wel, A., Noeske, K., Bezanson, R., et al. 2016, *ApJS*, 223, 29, doi: [10.3847/0067-0049/223/2/29](https://doi.org/10.3847/0067-0049/223/2/29)
- Vazdekis, A., Coelho, P., Cassisi, S., et al. 2015, *Monthly Notices of the Royal Astronomical Society*, 449, 1177, doi: [10.1093/mnras/stv151](https://doi.org/10.1093/mnras/stv151)
- Verde, L., Treu, T., & Riess, A. G. 2019, *Nature Astronomy*, 3, 891, doi: [10.1038/s41550-019-0902-0](https://doi.org/10.1038/s41550-019-0902-0)
- Wang, Y., Robberto, M., Dickinson, M., et al. 2019, *PASA*, 36, e015, doi: [10.1017/pasa.2019.5](https://doi.org/10.1017/pasa.2019.5)
- Zhang, C., Zhang, H., Yuan, S., et al. 2014, *Research in Astronomy and Astrophysics*, 14, 1221, doi: [10.1088/1674-4527/14/10/002](https://doi.org/10.1088/1674-4527/14/10/002)

APPENDIX

A. ASSESSING THE DEPENDENCE ON THE SPS MODEL

To verify the dependence of our results on the assumed stellar population synthesis (SPS) model, we repeat the entire analysis by adopting the α -MILES models by Vazdekis et al. 2015 (hereafter V15). Similarly to TMJ11, they are generated with variable age, $[Z/H]$, $[\alpha/Fe]$ parameters and use an updated version of the same empirical stellar library (MILES, Falc3n-Barroso et al. 2011), but are based on corrections from theoretical stellar spectra and assume different stellar isochrones (BaSTI, Pietrinferni et al. 2006). We note that with respect to TMJ11, one of the drawbacks of V15 models is that they allow a poorer exploration of the parameter space, having, in particular, a smaller sampling of $[\alpha/Fe] = 0, 0.4$. This introduces some limitations in their use, as will be discussed below, and is one of the reasons why we adopted TMJ11 models as our reference. On the other side, they give us the possibility to go a step further in the analysis of stellar population properties and test the assumption of a more extended star formation history (SFH \equiv SFR(t)). In particular, we adopt an exponentially declining function:

$$\text{SFR}(t) \propto e^{-(\text{age}-t)/\tau}, \quad (\text{A1})$$

where τ is the characteristic star formation timescale.

The following analysis closely follows the approach adopted in Paper I to measure indices in the observed data, the reader may refer to section 3 for further details. We generate synthetic spectra¹ with variable age, $[Z/H]$, $[\alpha/Fe]$ and τ covering the wavelength range $3550 < \lambda/\text{\AA} < 5500$ at a resolution of 2.5 \AA FWHM and measure the main spectral indices with pyLick². The original grid, spanning the following parameter space: $0.1 < \text{age}/\text{Gyr} < 14$ (14 points), $0.01 < \tau/\text{Gyr} < 3$ (7 points), $-2.25 < [Z/H] < 0.40$ (7 points), and only two $[\alpha/Fe]$ points (0 and 0.4), has been interpolated to a resolution of 0.2 Gyr in age and τ , and 0.02 dex in $[Z/H]$ and $[\alpha/Fe]$. This procedure does not introduce significant differences in the resulting parameters. As in the main analysis, we focus on the *baseline* set of spectral indices ($H\delta_A$, CN_1 , CN_2 , $Ca4227$, $G4300$, $H\gamma_A$, $H\gamma_F$, $Fe4383$, $Fe4531$, C_24668 , see Sect. 2), which allows us to maximize the number of constrained galaxies. The indices measured on modeled spectra, which are a function of $\theta = (\text{age}, \tau, [Z/H], [\alpha/Fe])$, are compared to the ones measured on the LEGA-C DR2 spectra at 2.5 \AA FWHM and corrected to zero velocity dispersion. Specifically, we adopt an MCMC approach using a log-likelihood function $\ln \mathcal{L} = (-1/2) \sum_i (I_i - I_i^{\text{mod}}(\theta))^2 / \sigma_i^2$ where I_i and σ_i refer to the index and its associated uncertainty. In the results presented here, we explore the entire parameter space allowed from the models and - we emphasize here - no cosmological priors are used to derive galaxy ages.

At the end of this process, we obtain two datasets describing the stellar population properties of the 140 cosmic chronometers using the V15 models:

1. V15 – SSP: single-burst SFH ($\tau \equiv 0$);
2. V15 – τ -dec: exponentially declining SFH (Eq. A1).

In the following section these we will be compared the TMJ11 results. For the purposes of this study, we are interested to detect any possible variation in the trends with redshift (which, as described in Eq. 1, is the quantity needed to constrain $H(z)$). In particular, we will discuss percentage differences in ages and absolute differences in $[Z/H]$ (already expressed in log units) as a function of z :

$$\eta = \text{age}_{\text{V15}}/\text{age}_{\text{TMJ11}} - 1, \quad \Delta = [Z/H]_{\text{V15}} - [Z/H]_{\text{TMJ11}}. \quad (\text{A2})$$

We note here that the interpolation between the two available $[\alpha/Fe]$ points is not optimal to capture the granularity of this parameter. Indeed, for almost all the galaxies ($> 90\%$), we obtain typical $[\alpha/Fe] \sim 0$, which is also the grid-point nearest to the values obtained with TMJ11 models (~ 0.13 dex). We have also checked that the *baseline* index

¹ We use the web tools available at: <http://research.iac.es/proyecto/miles/pages/webtools/tune-ssp-models.php> and <http://research.iac.es/proyecto/miles/pages/webtools/get-spectra-for-sfhs.php>

² Available at: <https://gitlab.com/mmoresco/pylick/>

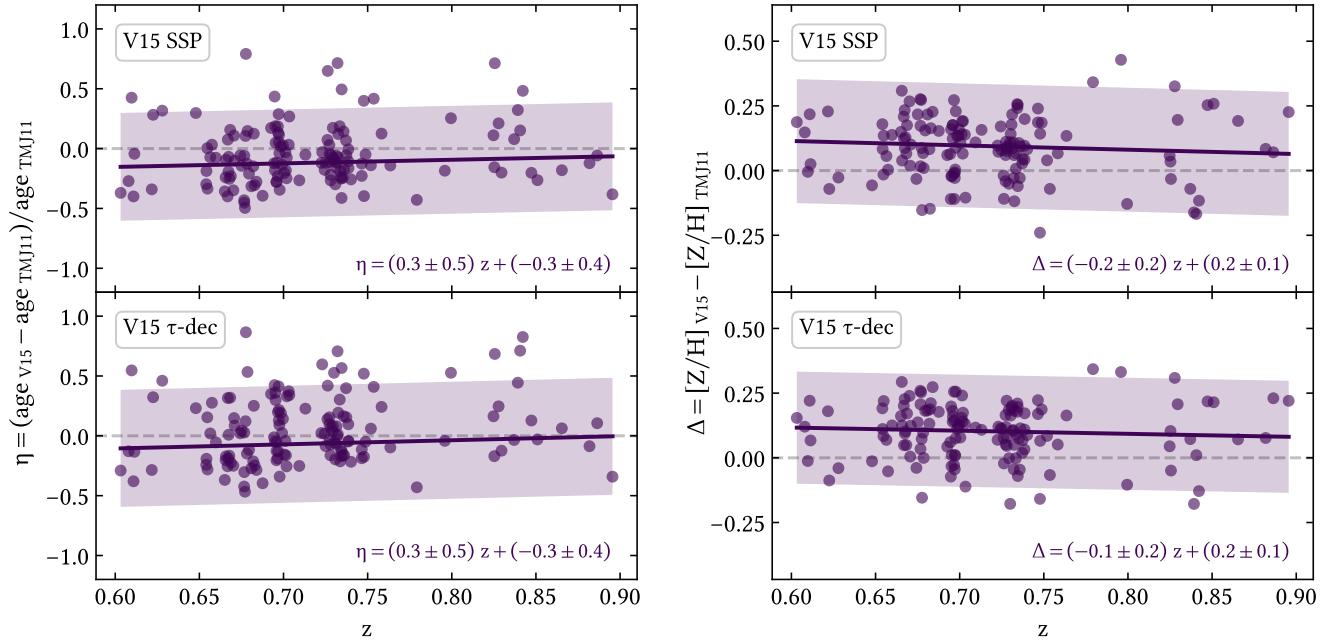


Figure 5. Differences as a function of redshift between stellar ages and metallicities of 140 LEGA-C passive galaxies obtained with Vazdekis et al. (2015) single-burst (SSP) and exponentially-declining (τ -dec) star formation histories versus Thomas et al. (2011) SSP models. Violet lines and shaded regions are robust linear fits and associated 2σ scatter regions, respectively.

combination is not optimal to capture $[\alpha/\text{Fe}]$ variations with the current models. While further analysis with models with denser $[\alpha/\text{Fe}]$ grid-points is needed to better understand these differences and study any possible trend of $[\alpha/\text{Fe}]$ with redshift, the analysis of age and $[\text{Z}/\text{H}]$ - which can be strongly degenerate - is sufficient to explore systematic effects on the final $H(z)$ value.

A.1. Different model with the same (single-burst) SFH

When galaxies are modeled as SSPs, we obtain typical values of $\langle \text{age} \rangle = 2.65 \pm 0.46$ Gyr and $\langle [\text{Z}/\text{H}] \rangle = 0.16 \pm 0.27$ dex, differing by -0.36 Gyr and $+0.08$ dex, respectively, from the results obtained with TMJ11. Even if these differences are consistent within 1σ , it is interesting to note that they follow the trend expected from the age-metallicity degeneracy, i.e. younger ages and higher metallicities. However, one of the main advantages of the cosmic chronometer method is that it is insensitive to any systematic offset of the age redshift relation (Eq. 1). We thus explore systematics studying the evolution of differences over redshift (Fig. 5, upper panels).

It is remarkable that we find no significant deviations as a function of z in the redshift range of interest, with typical differences ranging between $-0.15 < \eta < -0.07$ (with 0.22 rms scatter) and $0.07 < \Delta < 0.12$ (with 0.12 rms scatter). This means that the mean trends of this population of galaxies do not significantly deviate from those observed with TMJ11 models. As done in the main analysis of this Letter (§ 3), we compute age-redshift relations for the lower and the higher σ_* sub-samples in 4 redshift bins. The final $H(z)$ measurements using median and mean as estimators differ by only 0.6σ from the baseline. When also testing different binning schemes (including the systematic effects already estimated in Sect. 3.1), we obtain measurements consistent within 0.7σ .

A.2. Different model with a more extended (exponentially declining) SFH

In the main analysis of this Letter, we adopt a single-burst star formation history. Even if our selection criteria were chosen to obtain a sample of galaxies with very short SFH, the single single-burst approximation is not realistic. However, it is important to stress that any constant star formation time-scale for the entire population of these galaxies, leads to a vertical shift of the age-redshift relation, therefore the final $H(z)$ measurement would not be affected. Again, we want to test whether there is any trend of τ with z , which could in principle introduce a bias in the $H(z)$ measurement. At the same time, this analysis gives us the possibility to test how well our assumption of single-burst SFH fits with the observed sample.

Despite the wide range of τ adopted (0.01–3 Gyr), we obtain typical values of $\langle\tau\rangle = 0.24 \pm 0.21$ Gyr with only 23% of the galaxies having $\tau > 1$ Gyr. This is an important confirmation that the stellar components of the bulk of these systems formed in very short episodes. We also find no significant dependence on z , suggesting minor systematic effects on the final $H(z)$ value. From a more detailed analysis of their posterior distributions, we find that especially systems with $\tau \gtrsim 1$ Gyr suffer from strong degeneracy between age and τ . This degeneracy is well-known in the literature (e.g. Gavazzi et al. 2002) and together with the age-metallicity degeneracy is one of the major obstacles in the accurate reconstruction of galaxy star formation histories. Quantitatively, from the analysis of the posterior distributions of our dataset, we find:

$$\frac{\Delta\tau}{\Delta\text{age}} \simeq 0.3 \quad (\text{A3})$$

i.e., the same set of indices can be reproduced if a galaxy is 1 Gyr older and its star formation time scale extends by 0.3 Gyr. This aspect should be carefully considered when ages from different samples with different SFH assumptions are compared. The age-star formation timescale degeneracy is generally (partially) broken by placing a cosmological prior in the form of an upper limit on galaxies ages depending on the redshift of observation. However, we shall not use cosmological assumptions in our analysis, as it would introduce a circularity: the retrieved $H(z)$ constraints would be driven by the priors assumed. A possible solution could come from the detailed modeling of CaII H and K features, which have proven to be good diagnostics of underlying young stellar populations (see e.g. Moresco et al. 2018; Borghi et al. 2021). This can also be seen in Fig. 6 where we show a typical galaxy for which the best fit (blue curve, with $\tau = 1$ Gyr and age = 5 Gyr) provides similar results with respect to the solution with $\tau = 0.01$ Gyr and age = 3.5 Gyr (red curve). The spectral indices are insensitive to any difference in the flux normalization, therefore the normalization of models adopted in the figure (currently chosen in the range $4180 < \lambda/\text{\AA} < 4220$) is only used for a visual comparison of the models. On the contrary, the difference in the CaII H and K lines (not used in this analysis), could be a viable option, preferring the solution with lower τ . This diagnostic will be further explored in future work using the full spectral fitting technique, which allows more flexibility and extensibility to study galaxy SFHs. In this work, we repeat the analysis by fixing an upper prior of $\tau < 0.5$ Gyr corresponding to the upper 1σ value of the entire population. We verified that this prior does not significantly modify the shape of the age-redshift relation.

We obtain typical values of $\langle\text{age}\rangle = 2.88 \pm 0.61$ Gyr, $\langle\tau\rangle = 0.17 \pm 0.09$ Gyr and $\langle[Z/H]\rangle = 0.21 \pm 0.24$ dex, differing by +0.23 Gyr, +0.17 Gyr, and +0.05 dex, respectively, from the SSP results. In Fig. 5 (*lower panels*) we show the evolution of age and $[Z/H]$ differences over redshift.

Again, it is remarkable that there are no significant deviations as a function of z in the redshift range of interest, with typical differences ranging between $-0.11 < \eta < -0.01$ (with 0.24 rms scatter) and $0.08 < \Delta < 0.12$ (with 0.11 rms scatter). As in the main analysis of this Letter, we have computed median age-redshift relations for the lower and the higher σ_* sub-samples in 4 redshift bins. The final $H(z)$ measurements using median and mean as estimators differ by 0.8σ from the ones obtained with V15 assuming a single-burst SFH and by 0.4σ from the baseline (TMJ11, single-burst SFH). Also in this case, we test different binning schemes, obtaining measurements consistent within 0.7σ .

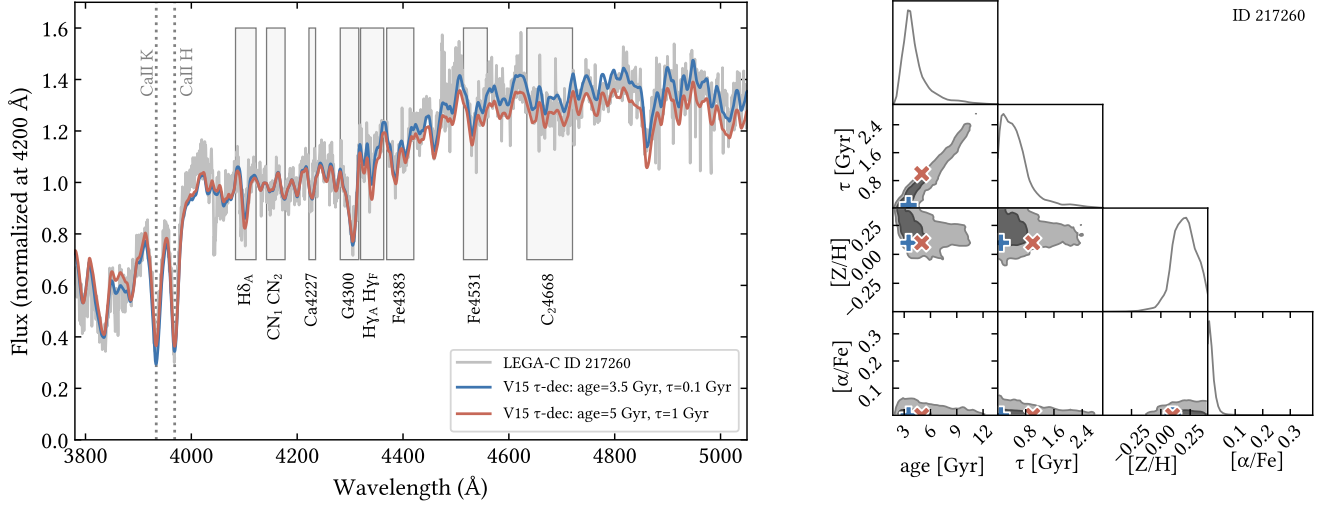


Figure 6. Example of age-star formation timescale degeneracy for a LEGA-C galaxy (ID 217260, $S/N \simeq 22 \text{ pix}^{-1}$) comparing the *baseline* index set (left plot, gray boxes) to the [Vazdekis et al. \(2015\)](#) τ -declining models. *Left:* Observed (gray) and synthetic (blue and red) spectra normalized at 4200 \AA . The blue spectrum corresponds to the model closer to the best-fit parameters, while the red one is taken at the edge of the 1σ confidence region. *Right:* Corner plot for stellar age, star formation timescale τ , stellar metallicity $[Z/H]$, and $[\alpha/Fe]$. The contours enclose 1σ (darker shade) and 2σ (lighter shade) confidence regions. Blue and red symbols indicate the values at which the synthetic spectra are generated.